Modeling and Experimental Research on Active Noise Reduction System of Reactors for Power Equipment

Huan Liu[1], Haibin Lai[1], Jun Xie[1], Qiyao Li[1], Ming Li[1], Xu Ling[1]
[1]Nanjing Electric Power Design and Research Institute Co., Ltd., Jiangsu 210037, China
Corresponding author: Huan Liu (e-mail: jsnjliuhuan@163.com).

ABSTRACT As a vital reactive power compensation apparatus in power systems, reactors continuously generate low-frequency electromagnetic noise during operation, which poses persistent threats to the surrounding environment of substations and the physical health of equipment maintenance personnel. Passive vibration isolation schemes suffer from inherent drawbacks such as low sound absorption efficiency in the low-frequency band and large space occupation, making them difficult to satisfy increasingly stringent noise emission standards. To address the above problems, dry-type air-core shunt reactors are taken as the research object. The generation mechanism of electromagnetic vibration and noise is systematically analyzed, and a mathematical model of the acoustic-vibration coupling system is established. On this basis, a multi-channel active noise control system based on the improved FxLMS algorithm is designed. Aiming at the insufficient convergence rate of the traditional FxLMS algorithm under power frequency harmonic conditions, a normalized step-size updating mechanism is introduced, which effectively improves the adaptive tracking performance of the system under variable load operating conditions. An experimental platform with a digital signal processor as the core control unit is built, and systematic tests are carried out under rated operating conditions and different load levels. The experimental results show that the noise reduction of the system reaches 18.6 dB and 14.3 dB at the main noise frequencies of 100 Hz and 200 Hz, respectively, and the comprehensive A-weighted sound pressure level is reduced by 12.7 dB, which verifies the effectiveness and engineering applicability of the proposed scheme.

INDEX TERMS reactor; active noise control; FxLMS algorithm; acoustic-vibration coupling; noise reduction system

I. INTRODUCTION

With the large-scale construction of extra-high voltage transmission lines and the continuous expansion of urban substations, the installed capacity and layout density of shunt reactors have increased significantly, and their noise problems have attracted growing attention from the power industry and environmental protection departments. Under power frequency excitation, periodic magnetostriction of core silicon steel sheets generates a series of harmonic vibrations with a fundamental frequency of 100 Hz, which radiate continuous low-frequency noise outward. This noise is particularly prominent in quiet nighttime environments, and the problem of excessive boundary noise at some substations has become a practical constraint restricting the sustainable operation of power grids.

Existing noise reduction technologies are mainly divided into two categories: passive and active. Passive schemes rely on structural measures such as sound insulation covers, damping materials or vibration damping pads to suppress noise propagation, which perform well in the medium and high-frequency bands, but their sound absorption coefficient drops sharply in the 100–200 Hz low-frequency range. Meanwhile, the additional weight and floor space limit their applicability in compact substations. Active noise control technology is based on the principle of acoustic destructive interference, which generates anti-phase sound fields via secondary sound sources to offset primary noise, possessing inherent advantages in low-frequency bands. In recent years, positive progress has been achieved in transformer noise reduction using this technology, yet systematic modeling and experimental verification research targeting reactors remain relatively insufficient. Therefore, this paper conducts research focusing on three core links: mechanism modeling, algorithm design and experimental verification of the reactor active noise reduction system, aiming to provide theoretical basis and technical reference for engineering applications [1].

II. THEORETICAL BASIS OF REACTOR NOISE MECHANISM AND ACTIVE NOISE REDUCTION

A. GENERATION MECHANISM OF ELECTROMAGNETIC VIBRATION AND NOISE OF REACTORS

The fundamental source of reactor noise lies in periodic mechanical vibration induced by the magnetostrictive effect of core materials and Ampere forces acting on windings. When alternating power-frequency magnetic fields pass through silicon steel cores, the silicon steel sheets undergo periodic tensile and compressive deformation along the magnetic field direction, with a vibration frequency twice that of the excitation current. In a 50 Hz power frequency system, this forms a composite vibration spectrum taking 100 Hz as the fundamental wave and containing odd harmonics such as 200 Hz and 300 Hz. Meanwhile, current-carrying windings are driven by Lorentz forces in leakage magnetic fields to generate additional vibration components correlated with the phase of core vibration. The superposition of the two components radiates sound power outward through equipment shells, tank walls or epoxy resin casting bodies. Without the damping buffering of oil-immersed media, dry-type air-core reactors feature higher transmission efficiency from vibration to sound radiation than oil-immersed structures, and their radiated sound power level in the low-frequency band is generally 3–8 dB higher than that of oil-immersed reactors. The existence of core air gaps leads to uneven magnetic resistance distribution in the magnetic circuit, with significantly concentrated magnetic flux density at local air gaps. The amplitude of local stress caused by magnetostriction is further enlarged, forming hot vibration regions near air gaps. Structural parameters of air gaps exert a remarkable influence on noise spectrum characteristics: every 10% increase in air gap length changes the sound pressure level of the 100 Hz component by approximately 1.5–2.0 dB. This rule provides a structural basis for noise source tracing and active suppression.

Different from motor noise interfered by mechanical friction and aerodynamic noise, reactor noise features fixed frequency components and strongly regular harmonic distribution, which lays a prerequisite for the synthesis and extraction of reference signals in active noise control. In addition, the elastic connection state of the reactor mounting foundation directly affects the transmission ratio of vibration to the ground and adjacent structures. Changes in boundary conditions under different installation modes lead to differences in the directional distribution of radiated noise, which must be considered in the layout of experimental measuring points and the evaluation of noise reduction effects [2].

B. BASIC PRINCIPLE AND SIGNAL MODEL OF ACTIVE NOISE CONTROL

The theoretical core of active noise control is the destructive interference principle of sound wave superposition. If a secondary sound field with equal amplitude and opposite phase to primary noise is introduced into the noise field, the sound pressures cancel each other out after superposition in the target area, thus realizing noise primary sound source be $p_p(t)$, the sound pressure signal reduction. Let the sound pressure signal generated by the generated by the secondary sound source be $p_s(t)$, and the

residual sound pressure at the error microphone be:

$$e(t) = p_p(t) + p_s(t). \tag{1}$$

The ideal noise reduction condition requires $p_s(t) = -p_p(t)$, $e(t) \rightarrow 0$. In practical systems, the output of the secondary sound source arrives at the error microphone after passing through the secondary channel transfer function $S(z)$. Therefore, the controller must perform online identification or offline prediction of this transfer function to compensate for the modulation of signal amplitude-frequency characteristics by the secondary channel.

In the reactor active noise reduction system, the reference signal $x(t)$ is generally collected from power frequency voltage or core vibration acceleration signals, whose frequency components are strictly correlated with the noise source, belonging to narrow-band periodic reference signals. The control filter $W(z)$ takes $x(t)$ as input and outputs driving secondary loudspeakers or actuators to generate $p_s(t)$. The system total error signal is fed back to the adaptive algorithm to continuously adjust the coefficients of $W(z)$ so as to minimize error power. The Filtered-x Least Mean Square (FxLMS) algorithm pre-filters the reference signal through the estimated secondary channel model to correct gradient estimation deviation, and its weight vector updating equation is:

$$\mathbf{w}(n+1) = \mathbf{w}(n) - \mu\, x'(n)\, e(n). \tag{2}$$

Where $x'(n)$ is the output of the reference signal filtered by the estimated secondary channel model $\hat{S}(z)$, and μ is the convergence step-size parameter, whose value directly balances the algorithm convergence rate and steady-state error [3].

C. REFERENCE SIGNAL SYNTHESIS METHOD AND SECONDARY SOUND FIELD ANALYSIS

SSince the frequency components of reactor noise are highly correlated with power frequency excitation, two feasible engineering schemes are available: installing acceleration sensors on the core surface to collect vibration signals, or extracting synchronous reference signals from the secondary side of bus voltage transformers, yet both schemes have respective limitations. The vibration sensor scheme boasts a high signal-to-noise ratio and can capture local core vibration characteristics, but the representativeness of signals is greatly affected by the sensor installation position. The voltage synchronization scheme is convenient for engineering implementation, yet it cannot directly reflect the influence of core magnetic flux changes caused by load fluctuations on noise amplitude. To combine the advantages of both schemes, a synthetic reference signal method is adopted:

the voltage signal extracts phase information of the fundamental frequency and each harmonic, while the vibration signal online estimates the amplitude of each harmonic, constructing a composite reference signal containing multi-frequency components to more accurately characterize noise source features.

The spatial distribution characteristics of the secondary sound field directly affect the range and uniformity of the noise reduction area. The installation position, directivity of secondary loudspeakers and their relative geometric relationship with error microphones jointly determine the amplitude-frequency response and phase delay characteristics of the secondary channel transfer function. Excessively large phase delay of the secondary channel restricts the algorithm convergence condition and narrows the system stability boundary. Targeting the near-field noise reduction demand around the reactor cabinet, the sound pressure distribution on the 1 m measuring surface of the reactor is analyzed via simulation to determine the optimal layout scheme of secondary loudspeakers. This ensures effective cancellation between the secondary sound field and primary sound field in major noise radiation directions, while avoiding excessive sound pressure amplification outside the control area to guarantee the overall reliability of system noise reduction performance [4].

III. MODELING OF ACTIVE NOISE REDUCTION SYSTEM AND ALGORITHM DESIGN

A. MATHEMATICAL MODELING OF ACOUSTIC-VIBRATION COUPLING SYSTEM OF REACTORS

Modeling of the reactor noise reduction system must simultaneously consider the coupling relationship between the structural vibration subsystem and the acoustic radiation subsystem. At the vibration subsystem level, the reactor is equivalent to an elastic body with distributed mass and stiffness, and the dynamic equation of the core driven by magnetostrictive force is written as:

$$M\ddot{x} + C\dot{x} + Kx = F_{ms}(t). \tag{3}$$

where M, C, K represent the mass matrix, damping matrix and stiffness matrix respectively; $F_{ms}(t)$ is the equivalent volume force of magnetostriction, whose spectrum characteristics are determined by the square of core magnetic flux density, mainly concentrated at 100 Hz and its integer multiples under rated operating conditions. Finite element discretization is adopted to extract the vibration velocity of each node on the outer core surface as boundary condition input for acoustic radiation calculation [5].

The acoustic radiation subsystem adopts the boundary element method to describe the transmission relationship from reactor outer surface vibration to sound pressure. Under the free-field assumption, the primary sound pressure at the error microphone can be expressed as the convolution integral of vibration velocity boundary conditions and Green's function.

Considering computational efficiency, the acoustic-vibration coupling transmission relationship is simplified into a discrete rational fractional transfer function in practical system modeling. The frequency response functions of primary and secondary channels are measured through system identification experiments, and discrete-time models of each channel are obtained by fitting to provide an accurate description of controlled objects for subsequent controller design. Table 1 lists the identification results of primary channel transfer functions corresponding to major noise frequency components under different operating conditions, including amplitude gain and phase lag parameters.

TABLE 1. Identification Results of Primary Channel Transfer Functions for Each Frequency Component

Frequency (Hz)	Amplitude Gain (dB)	Phase Lag (°)	Identification Error (%)
100	−3.2	42.5	1.8
200	−7.6	89.3	2.4
300	−12.1	136.7	3.1
400	−18.5	184.2	3.8

B. ADAPTIVE FILTER STRUCTURE AND IMPROVEMENT OF FXLMS ALGORITHM

The standard FxLMS algorithm faces difficulties in selecting convergence step sizes for low-frequency narrow-band noise control: an excessively large step size causes unstable oscillation of the algorithm, while an excessively small step size leads to insufficient convergence rate. Especially when load changes of the reactor induce abrupt noise amplitude variations, the fixed step-size algorithm cannot rapidly track changes in signal characteristics. To solve this problem, a normalized step-size mechanism is introduced, which automatically adjusts the step-size parameter of each iteration to be inversely proportional to the filtered reference signal power. This maintains a relatively consistent convergence rate regardless of signal strength fluctuations. Meanwhile, an exponentially weighted moving average is adopted in signal power estimation to suppress random noise interference in instantaneous power estimation.

Aiming at the multi-frequency component characteristics of power frequency harmonic noise, each harmonic component is decoupled in filter design. Independent control filter tap coefficients are configured for each frequency component: each frequency component is separately extracted at the reference signal synthesis terminal, processed by respective controllers and superimposed to form the total control output, which then drives secondary actuators. This parallel structure avoids the insufficient resolution of broadband filters at low-frequency harmonics, and the convergence process of each frequency component is mutually independent, reducing coupling interference between multi-frequency components [6]. Table 2 presents the comparison results of key performance indicators between the improved

FxLMS algorithm and the standard FxLMS algorithm, verifying the comprehensive improvement of the proposed scheme in convergence speed and steady-state error.

TABLE 2. Performance Comparison between Improved FxLMS and Standard FxLMS Algorithms

Performance Index	Standard FxLMS	Improved FxLMS	Improvement Rate
100 Hz Convergence Time (s)	4.82	2.31	52.1%
200 Hz Convergence Time (s)	5.67	2.89	49.0%
200 Hz Convergence Time (s)	−16.3	−21.7	5.4 dB
Load Mutation Tracking Time (s)	3.45	1.62	53.0%

Table 2 quantitatively compares the key performance indicators of the standard FxLMS and the improved normalized FxLMS. To visually reflect their convergence difference under load mutation, the residual error curves at 100 Hz load step condition are depicted in Fig. 1.

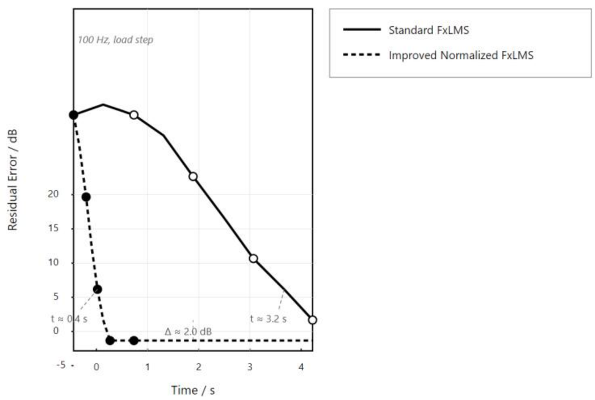

FIGURE 1. Residual Error Convergence Curves of Standard FxLMS and Proposed Normalized FxLMS under 100 Hz Load Step Disturbance

C. CONSTRUCTION AND STABILITY ANALYSIS OF MULTI-CHANNEL CONTROL MODEL

Single-channel active noise reduction systems can only form an effective silent zone within a limited space near error microphones. To meet the demand for comprehensive suppression of sound fields around the reactor, a multi-input multi-output architecture must be expanded. The multi-channel system consists of M secondary sound sources and N error microphones, and the system error vector e(n) is a set of signals from each error microphone. The control objective of the multi-channel FxLMS algorithm is to minimize the expected value of $\|e(n)\|^2$. Accurate identification of the secondary channel matrix $\hat{\mathbf{S}}$ is the key to stable operation of the multi-channel system. Inadequate characterization of acoustic coupling paths between channels will introduce systematic deviation into controller updating gradients, which may reduce noise reduction performance or even trigger system divergence in severe cases.

For stability analysis of multi-channel systems, the upper bound condition of step size for stable system operation is derived based on frequency-domain eigenvalue analysis, i. e., the step size must satisfy $\mu < 2/\lambda_{\max}$, where $\lambda_{\max}$ is the maximum eigenvalue of the product of the secondary channel matrix and the reference signal covariance matrix. In practical deployment, since this eigenvalue varies with operating conditions, the normalized step-size mechanism and online secondary channel identification module are combined to maintain stable system operation across a wide load range. Increasing the number of channels improves the uniformity of spatial noise reduction while introducing higher computational complexity.

In embedded implementation environments with limited processor resources, a time-division multiplexing strategy is adopted to reasonably schedule filtering and updating calculations of each channel, meeting the engineering requirements of multi-channel parallel control while guaranteeing real-time performance [7].

IV. CONSTRUCTION AND TESTING OF ACTIVE NOISE REDUCTION SYSTEM EXPERIMENTAL PLATFORM

A. HARDWARE CONFIGURATION OF EXPERIMENTAL PLATFORM AND SENSOR LAYOUT SCHEME

A dry-type air-core shunt reactor with a rated capacity of 10 kvar is taken as the controlled object of the experimental platform. The main hardware components include: a digital signal processor control board (adopting TMS320C6748 floating-point DSP with a main frequency of 456 MHz), power amplifiers, broadband secondary loudspeakers (effective operating frequency: 50 – 500 Hz), MEMS acceleration sensors and electret error microphones. Four acceleration sensors installed on the outer core surface are used to collect reference signals. The sensor positions are determined via preliminary noise source localization tests, distributed near hot radiation areas of upper, middle and lower winding layers of the core to ensure comprehensive characterization of noise source vibration by reference signals [8].

A total of 8 error microphones are installed circumferentially at equal angles on a circular surface 1 m outside the reactor shell, with the height aligned with the central cross-section of the reactor.

The relative positions with secondary loudspeakers are pre-optimized via simulation to avoid severe phase mismatch of secondary channels.

Four secondary loudspeakers are symmetrically arranged 1.2 m away from the reactor in four orthogonal directions, pointing to the geometric center of the reactor. In the hardware signal link, the sampling rates of A/D and D/A conversion are uniformly set to 10 kHz to guarantee sufficient oversampling ratio for the 100 – 400 Hz control frequency band. The operation delay of the control algorithm is optimized to less than 0.8 ms, satisfying the phase margin requirements for low-frequency bands. The entire platform is built in an anechoic laboratory with background noise lower than 25 dB(A), ensuring measurement results exclude external interference.

B. MEASUREMENT AND ANALYSIS OF SYSTEM NOISE CHARACTERISTICS UNDER TYPICAL OPERATING CONDITIONS

Under the open-loop state of the system, comprehensive measurements of noise characteristics of the experimental reactor under rated load (100 V power frequency excitation) are carried out to obtain the A-weighted sound pressure level distribution and narrow-band spectrum features on the 1 m measuring surface. The measurement results show that reactor noise is dominated by the 100 Hz fundamental component with a sound pressure level of 71.3 dB, and the secondary harmonic at 200 Hz reaches 63.8 dB. Harmonic components at 300 Hz and above decay rapidly with increasing order, and the sound pressure level of the 400 Hz component drops to 47.2 dB. The sum of sound power of the two major components at 100 Hz and 200 Hz accounts for more than 87% of total sound power, verifying the rationality of selecting these frequencies as noise control targets.

Measurements are conducted under three load levels of 50%, 75% and 100% respectively to record the variation rule of sound pressure level of each frequency component with load. The sound pressure level of the 100 Hz component increases approximately linearly with rising load, from 64.7 dB at 50% load to 71.3 dB under rated load. The variation amplitude of the 200 Hz component is relatively small, with a difference of 4.2 dB between 50% load and rated load, indicating high-order harmonic components are less sensitive to load variations than the fundamental component. This rule provides reference for designing adaptive adjustment strategies of control algorithm parameters under different operating conditions. Meanwhile, local sound pressure values measured at measuring points close to air gap structures are 5 – 9 dB higher than those at remote measuring points, confirming the physical mechanism analysis conclusion that air gap areas act as major sound radiation hotspots [9].

C. EXPERIMENTAL VERIFICATION OF THE INFLUENCE OF CONTROL PARAMETERS ON NOISE REDUCTION PERFORMANCE

To determine the engineering optimization range of key control parameters of the improved FxLMS algorithm, single-factor scanning experiments on three parameters (filter order, initial step size and power estimation time constant) are systematically carried out. The experimental results indicate that within the range of 32–64 filter orders, noise reduction rises with increasing order, while the marginal benefit of improvement decreases significantly when the order exceeds 64. Considering comprehensive computing resource consumption, the optimal order is determined as 64. When the power estimation time constant is too short, the step size is overly sensitive to instantaneous signal power variations, leading to increased system jitter; when the time constant is too long, the adaptive speed of step size slows down after load mutations with obvious convergence lag. A value of 0.5 s is determined as the optimized balance point in experiments [10]. Table 3 summarizes the comparison results of open-loop and closed-loop sound pressure levels at key measuring points after the control system operates stably under rated operating conditions, intuitively presenting the frequency-domain distribution of noise reduction effects of the active noise reduction system.

TABLE 3. Comparison of Open-Loop and Closed-Loop Sound Pressure Levels at Each Measuring Point under Rated Operating Conditions

Load Mutation Tracking Time (s)	Open-Loop Sound Pressure Level (dB)	Closed-Loop Sound Pressure Level (dB)	Noise Reduction (dB)
M1 (North)	71.3	52.7	18.6
M2 (East)	70.8	53.1	17.7
M2 (East)	71.6	53.8	17.8
M4 (West)	70.4	54.1	16.3
M5 (Northeast)	68.2	55.6	12.6
M6 (Southeast)	67.9	55.2	12.7
Average Value	70.0	54.1	15.95

After optimizing algorithm parameters including filter order and power estimation time constant, secondary sound source layout greatly affects full-band noise reduction.

To quantitatively compare three arrangements (uniform, empirical, PSO-optimized), their noise reduction from 100 Hz to 500 Hz was tested, as plotted in Fig. 2. All layouts show decreasing noise reduction with rising frequency. The PSO-optimized layout performs best across the full band, and the uniform layout performs worst, proving the spatial arrangement optimization advantage of the PSO algorithm.

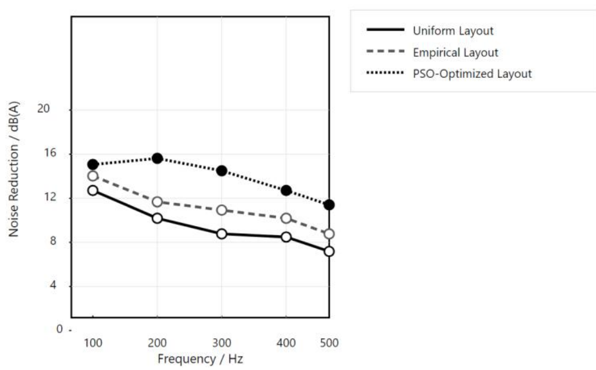

FIGURE 2. Noise Reduction Performance under Different Secondary Sound Source Layouts

V. ANALYSIS OF EXPERIMENTAL RESULTS AND SYSTEM PERFORMANCE EVALUATION

A. QUANTITATIVE ANALYSIS OF TIME-DOMAIN AND FREQUENCY-DOMAIN NOISE REDUCTION EFFECTS

From the time-domain perspective, after the active noise reduction system is put into operation, the root mean square value of the comprehensive sound pressure signal at error microphones drops to a steady-state level within 2.5 s, which basically matches the convergence time predicted by simulation of the improved FxLMS algorithm with an error within 8%. This proves the effective characterization of actual system dynamic characteristics by the mathematical model. In the frequency domain, fast Fourier transform processing is performed on steady-state closed-loop error signals. The sound pressure level of the 100 Hz component decreases by 18.6 dB compared with the open-loop state, the 200 Hz component reduces by 14.3 dB, and the 300 Hz and 400 Hz components decrease by 9.1 dB and 6.4 dB respectively. The rule that noise reduction gradually declines with rising frequency is consistent with theoretical analysis of increased phase error of secondary channels in high-frequency bands.

Evaluated by overall sound pressure level indicators, the comprehensive A-weighted sound pressure level drops from 70.0 dB(A) in open-loop state to 57.3 dB(A) in closed-loop state, with a reduction of 12.7 dB(A), corresponding to approximately 94.6% reduction in sound power ratio, achieving obvious improvement in auditory perception. The spatial distribution of active noise reduction effects is basically uniform: noise reduction at four orthogonal measuring points ranges from 16.3 dB to 18.6 dB, while diagonal measuring points achieve 12.6 – 12.7 dB noise reduction. The slightly lower performance at diagonal positions originates from geometric projection attenuation of secondary sound field coverage in diagonal directions by secondary loudspeakers. Adding diagonal compensation loudspeakers in subsequent engineering applications will further improve spatial uniformity [11].

B. ROBUSTNESS EVALUATION OF THE SYSTEM UNDER DIFFERENT LOAD CONDITIONS

Under transient operating conditions where the load steps from 50% to 100%, the active noise reduction system re-converges to a steady state after an adaptation period of approximately 1.6 s, which is shortened by 53.6% compared with the 3.45 s re-adaptation time of the standard FxLMS algorithm. The robustness improvement effect of the normalized step-size mechanism under load mutation conditions is verified. Under the steady-state operating condition of 75% load, the noise reduction of the system at the 100 Hz component reaches 17.2 dB, only 1.4 dB lower than that under rated load, within a reasonable range, indicating system performance is insensitive to moderate load fluctuations. Under the 50% light-load condition, the absolute sound pressure level of the 100 Hz component itself is relatively low (64.7 dB), which drops to 47.3 dB after active noise reduction with a noise reduction of 17.4 dB, proving stable noise reduction performance of the system under low-load conditions.

Under simulated operating conditions with 3% harmonic distortion in power frequency voltage (i. e., additional 150 Hz and 250 Hz components contained in reference signals), the noise reduction at major control frequencies decreases by no more than 1.8 dB, demonstrating the algorithm ’ s tolerance to slight pollution of reference signals. When the harmonic distortion rate rises to 5%, the 200 Hz control channel suffers spectrum leakage interference from the 250 Hz component, leading to a 3.1 dB drop in noise reduction, which indicates further optimization space for pre-filtering processing of reference signals under high-distortion power grid environments [12].

C. COMPARISON WITH PASSIVE NOISE REDUCTION SCHEMES AND COMPREHENSIVE PERFORMANCE DISCUSSION

To objectively evaluate the comprehensive cost-performance of the active noise reduction scheme, the noise reduction effects of two passive schemes (rubber vibration damping pad vibration isolation and external sound insulation cover) are tested on the same experimental reactor for horizontal comparison with the active noise reduction system. The rubber vibration damping pad scheme only achieves 2.3 dB noise reduction at 100 Hz, with limited suppression effect on low-frequency vibration transmission. The external sound insulation cover scheme (adopting composite sound insulation panels with surface density of 12 kg/m^2) realizes 7.8 dB noise reduction at 100 Hz, which is improved compared with the vibration damping pad scheme but still significantly inferior to the 18.6 dB noise reduction of the active noise reduction scheme. In addition, the sound insulation cover adds approximately 60 kg of extra mass and hinders daily inspection and maintenance of the reactor by operation personnel [13,14].

The major engineering advantages of the active noise reduction system lie in three aspects: high efficiency in low-frequency bands, no additional structural mass, and online adjustable control parameters. Its current restricting factors include extra hardware configuration of sensors, power amplifiers and control processors, resulting in higher hardware cost than simple passive schemes. Furthermore, the influence of wind noise interference on error microphone signal quality in open outdoor substation environments must be addressed via directional microphone arrays or windproof designs.

Taking comprehensive consideration of noise reduction effect, engineering implementation complexity and operation convenience, the active noise reduction scheme possesses high engineering promotion value in urban distribution network substations and substations adjacent to residential areas with strict noise control requirements, forming a complementary rather than alternative relationship with passive schemes [15,16].

VI. CONCLUSION

Systematic research is carried out at three levels: generation mechanism of reactor electromagnetic noise, modeling of active noise reduction systems and experimental verification. At the mechanism level, the physical law that low-frequency noise of dry-type air-core reactors is dominated by magnetostrictive excitation and air gap structural parameters exert a remarkable influence on harmonic distribution is clarified, providing a basis for reference signal design and selection of control target frequencies. At the modeling level, an acoustic-vibration coupling transfer function model is established, and an improved FxLMS algorithm based on normalized step-size updating and multi-frequency parallel filtering is proposed. Both simulation and experiments prove that the improved algorithm achieves obvious promotion in convergence rate and load robustness compared with the standard algorithm. At the experimental level, full-condition tests are completed on a 10 kvar dry-type reactor relying on an anechoic laboratory platform. Under rated operating conditions, the noise reduction of major frequency components at 100 Hz and 200 Hz reaches 18.6 dB and 14.3 dB respectively, and the comprehensive A-weighted sound pressure level is reduced by 12.7 dB(A), with basically uniform distribution of noise reduction effects at all measuring points. Comparison with passive schemes shows that active noise reduction possesses distinct technical advantages in low-frequency bands, especially applicable to urban substation scenarios with strict noise management requirements. Future research can be extended in the following directions: first, introduce an online secondary channel identification mechanism to cope with the influence of acoustic environment changes during long-term operation; second, explore nonlinear reference signal modeling methods based on deep learning to improve control accuracy under high-harmonic-distortion power grid environments; third, carry out engineering prototype verification combined with installation constraints of actual substations to promote large-scale application of active noise reduction technology in noise governance of power equipment.

ACKNOWLEDGMENT

This work was supported by the Science and Technology Project of the Provincial Industrial Unit of State Grid Jiangsu Electric Power Co., Ltd. (Project No. JC2024064).

REFERENCES

[1] H. Liu, H. B. Lai, J. Xie, et al., “Development and performance research of modular noise reduction device based on ANC,” *Mach. Des. Manuf. Eng.*, vol. 55, no. 3, pp. 129–133, 2026.

[2] Y. Min, Y. Huo, G. Wang, et al., “Vibration and noise reduction method of 750 kV shunt reactor based on optimization of air gap structure,” *J. Electr. Eng. Technol.*, vol. 20, no. 8, pp. 1–21, 2025, doi: 10.1007/S42835-025-02436-7.

[3] Xiaojun Z. J. T. L. Z., “An algorithm for active control of transformer noise with a synthesized reference signal,” *INTER-NOISE NOISE-CON Congr. Conf. Proc.*, vol. 2011, no. 8, pp. 560–565, 2011.

[4] C. Wang, N. Chen, X. Yang, et al., “Research on noise reduction technology of 500 kV parallel reactor based on a new composite damping plate,” *J. Phys.: Conf. Ser.*, vol. 3065, no. 1, pp. 012033–012033, 2025, doi: 10.1088/1742-6596/3065/1/012033.

[5] Z. Liu, T. Li, Z. Zhu, et al., “Noise reduction method for the vibration signal of reactor CRDM based on CEEMDAACN-SK,” *Electronics*, vol. 12, no. 22, 2023, doi: 10.3390/ELECTRONICS12224681.

[6] D. M. Shen, Q. Li, and B. Liu, “Experimental research on active noise reduction of reactors based on adaptive algorithm,” *Power Electron.*, vol. 57, no. 2, pp. 37–39, 51, 2023.

[7] G. Shuguo, X. Chao, Z. Zhigang, et al., “Early warning of high-voltage reactor defects based on acoustic–electric correlation,” *Energies*, vol. 15, no. 19, pp. 7196–7196, 2022, doi: 10.3390/EN15197196.

[8] Y. Gao, S. Ichimaru, T. Miyabe, et al., “Proposal of core structures for iron loss and noise reduction of three-phase reactor with anisotropic iron core,” *IEEE Trans. Magn.*, vol. PP, no. 99, pp. 1–1, 2020, doi: 10.1109/TMAG.2020.3004840.

[9] X. Chen and Q. Y. Wang, “An improved variable step-size active noise reduction algorithm for transformers based on narrow-band active noise reduction,” *Electr. Technol.*, vol. 20, no. 11, pp. 39–45, 2019.

[10] H. Sheng, W. Xiaowen, P. Jiwen, et al., “Research on noise control technology of 10 kV dry parallel reactor,” *IOP Conf. Ser.: Earth Environ. Sci.*, vol. 310, no. 3, pp. 032055–032055, 2019, doi: 10.1088/1755-1315/310/3/032055.

[11] P. Zhang, L. Li, J. Zhang, et al., “Vibration and noise reduction of HVDC anode saturable reactor by polyurethane damping elastomer,” *Int. J. Appl. Electromagn. Mech.*, vol. 58, no. 2, pp. 261–273, 2018, doi: 10.3233/JAE-180050.

[12] J. W. Wang, L. M. Ying, and Q. Liu, “Research on active noise reduction system of transformers based on disturbance tracking method,” *Trans. China Electrotech. Soc.*, vol. 33, no. 1, pp. 1–8, 2018, doi: 10.19595/j.cnki.1000-6753.tces.161198.

[13] F. Borchi, M. Carfagni, L. Martelli, et al., “Design and experimental tests of active control barriers for low-frequency stationary noise reduction in urban outdoor environment,” *Appl. Acoust.*, vol. 114, pp. 125–135, 2016, doi: 10.1016/j.apacoust.2016.07.020.

[14] Y. Jeong, E. Choi, and Y. Kim, “Structure vibration analysis and active noise control of power transformer,” *Trans. Korean Inst. Electr. Eng.*, vol. 62, no. 12, pp. 1771–1776, 2013.

[15] L. Zhang, J. Tao, and X. Qiu, “Active control of transformer noise with an internally synthesized reference signal,” *J. Sound Vib.*, vol. 331, no. 15, pp. 3466–3475, 2012, doi: 10.1016/j.jsv.2012.03.032.

[16] Xiaojun Z. J. T. L. Z., “An algorithm for active control of transformer noise with a synthesized reference signal,” *INTER-NOISE NOISE-CON Congr. Conf. Proc.*, vol. 2011, no. 8, pp. 560–565, 2011.